# Non-intrusive and Efficient Estimation of Antenna 3-D Orientation for WiFi APs

Dawei Yan, Panlong Yang, *Senior Member, IEEE*, Fei Shang,
Nikolaos M. Freris, *Senior Member, IEEE*, and Yubo Yan, *Member, IEEE*

*Abstract*—The effectiveness of WiFi-based localization systems heavily relies on the spatial accuracy of WiFi AP. In real-world scenarios, factors such as AP rotation and irregular antenna tilt contribute significantly to inaccuracies, surpassing the impact of imprecise AP location and antenna separation. In this paper, we propose *Anteumbler*, a non-invasive, accurate, and efficient system for measuring the orientation of each antenna in physical space. By leveraging the fact that maximum received power occurs when a Tx-Rx antenna pair is perfectly aligned, we build a spatial angle model capable of determining antennas' orientations without prior knowledge. However, achieving comprehensive coverage across the spatial angle necessitates extensive sampling points. To enhance efficiency, we exploit the orthogonality of antenna directivity and polarization, and adopt an iterative algorithm, thereby reducing the number of sampling points by several orders of magnitude. Additionally, to attain the required antenna orientation accuracy, we mitigate the influence of propagation distance using a dual plane intersection model while filtering out ambient noise. Our real-world experiments, covering six antenna types, two antenna layouts, two antenna separations ($\lambda/2$ and $\lambda$), and three AP heights, demonstrate that *Anteumbler* achieves median errors below $6°$ for both elevation and azimuth angles, and exhibits robustness in NLoS and dynamic environments. Moreover, when integrated into the reverse localization system, *Anteumbler* deployed over LocAP reduces antenna separation error by $10\,\text{mm}$, while for user localization system, its integration over SpotFi reduces user localization error by more than $1\,\text{m}$.

*Index Terms*—WiFi localization, Antenna orientation, Polarization matching.

## I. INTRODUCTION

**W**IFI is developing as a candidate for indoor sensing for its low cost and ubiquitous infrastructure. Many works utilise WiFi devices to achieve fine-grained sensing tasks, such as localization and tracking [1]–[4], health monitoring [5], [6] and object imaging [7]–[10]. Despite previous research demonstrating the great potential of WiFi sensing, the direct application of existing schemes to sense indoor environments remains a rather challenging problem. A major reason is the need to ensure the credibility of the WiFi infrastructure itself, *i.e.*, the requirement for accurate prior knowledge of WiFi *access points'* (APs') or antennas' locations and orientations in the sensing ambiences. Inaccuracies in this knowledge may introduce computational errors that render the sensing systems

D. Yan, F. Shang, N. Freris, and Y. Yan are with School of Computer Science and Technology, University of Science and Technology of China, Hefei 230021, China. (e-mail: yandw@mail.ustc.edu.cn, shf_1998@outlook.com, yuboyan@ustc.edu.cn, nfr@ustc.edu.cn). P. Yang is with School of Computer Science, Nanjing University of Information Science & Technology, Nanjing 210044, China.(e-mail: plyang@ustc.edu.cn).
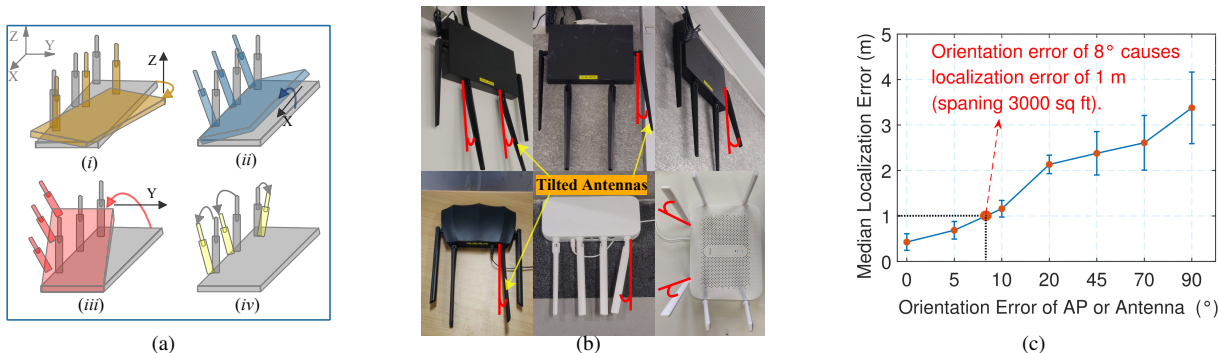
P. Yang and Y. Yan are the corresponding authors.

ineffective [11]. For example, techniques that use antenna arrays to combat multipath rely on precise antenna separation and orientation [1]–[3], and feature-based sensing methods require that the antennas remain relatively consistent during the training and inference [12], [13].

Moreover, the polarization of the antenna plays an important role in wireless communication and sensing. Although there are some researches devoted to the use of circularly polarized antennas for indoor localization and communication to better combat indoor complex environments [14]–[16], there are still few deployments in practice. At present, dipole antennas and monopole antennas are commonly used at APs and *Internet of Things* (IoT) devices, and these antennas are omnidirectional and linearly polarized [17]–[19]. Two such antennas perform best when they are oriented in parallel, and perform poorly when they are perpendicular to each other which, in turn, affects communication and sensing range [20], [21].

To specify this issue, this paper take WiFi localization as a case and examines how the credibility of WiFi infrastructure affects accuracy. In WiFi localization, WiFi APs can calculate the exact position of user based on *Received Signal Strength Indicator* (RSSI), *Channel State Information* (CSI), *Angle of Arrival* (AoA) or *Time of Flight* (ToF). Such localization systems require prior knowledge of the positions and orientations of WiFi AP or its antenna array in indoor map. These spatial properties can of course be obtained manually and calibrated regularly, but are obviously very time consuming and labor-intensive, especially when there are many WiFi APs. In particular, antenna orientation is an often overlooked aspect. Nevertheless, errors in antenna orientation can lead to decreased accuracy in the localization system [18], [22]–[24]. In real scenarios, as shown in Fig. 1a and Fig. 1b, due to manual measurement errors during deployment or the pursuit of higher throughput [25], [26], the tilt of the AP or antenna orientation is common, and they may have four orientation errors (*i.e.*, yaw, roll, pitch, irregular tilt). It's worth mentioning that inaccuracies in WiFi AP's or antenna's orientation are more important than inaccuracies in AP location and antenna separation. Specifically, it takes $30\,\text{cm}$ of AP position drift to introduce $50\,\text{cm}$ of localization error [24], and typically only the exposed antennas' separations may change. In contrast, according to our test in a scenario that spans $3000\,\text{sq\,ft}$ in area, an orientation error of $8°$ causes a localization error of $1\,\text{m}$, as shown in Fig. 1c. *The reasons for orientation error and the impact on localization systems are detailed in Section II.*

Thus, precise measurement of the orientations of all APs' antennas is anticipated to greatly facilitate the widespread

Fig. 1: **Motivation for *Anteumbler*:** (a) Four orientation errors of AP or antennas (yaw, roll, pitch, irregular tilt). (b) The antennas of AP have different tilted angles in real scenarios. (c) The localization error *vs.* the orientation error of AP or antenna.
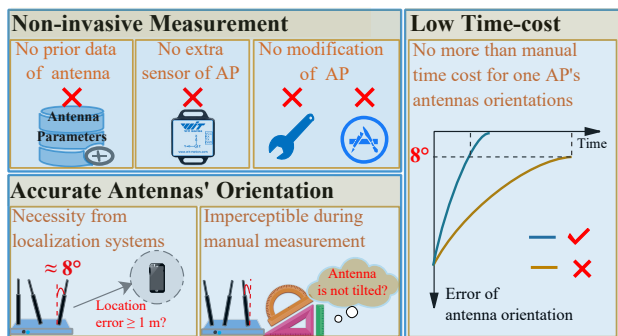


Fig. 2: **A system that measures the antennas orientations of WiFi APs should meet three requirements.**

implementation of various WiFi-based localization systems in real-world scenarios, ensuring sustained high accuracy over time. For instance, regularly reporting the orientations of all WiFi APs' antennas within a given area can inform calibration strategies. Specifically, in cases where AP antennas are uniformly tilted (yaw, roll, pitch), localization systems utilize the reported antenna orientations to accurately locate users. Conversely, when antennas are irregularly tilted, targeted calibration efforts require less manpower compared to aimless calibration. Another more obvious effect is for the localization systems to better estimate the user's location by compensating for the antenna parameters based on the reported actual orientations of the antennas.

As shown in Fig. 2, such a system for measuring the antennas orientations should satisfy the following requirements:

- **Non-invasive measurement.** The system should be capable of measuring the orientations of WiFi APs antennas within an unfamiliar environment. Crucially, this process should not rely on prior information about the antennas, require additional sensors like gyroscopes or cameras on the APs, or necessitate any hardware or firmware modifications to the APs.
- **Accurate antennas' orientations.** Our objective is to achieve a localization error of less than $1\,\mathrm{m}$ within an area equivalent to $3000\,\mathrm{sq\,ft}$. Therefore, considering the impact of antenna orientation errors on localization accuracy as depicted in Fig. 1c, the system's antenna orientation prediction error should be no greater than $8\,°$.
- **Low time-cost.** The system should efficiently measure the orientations of AP antennas, particularly in scenarios with thousands of APs, ensuring the measurement time

does not exceed that of manual measurement. For instance, based on our survey findings, manually measuring the orientations of four antennas on a single AP typically takes several minutes.

Unfortunately, to the best of our knowledge, most current systems cannot satisfy all of the above requirements simultaneously. Generally, there are following methods to measure antenna orientation: *(i)* The manual solutions are time-consuming, laborious, and prone to human error [27]; *(ii)* The sensor-based methods require special sensors to be installed on the antenna, which is inconvenient [28], [29]; *(iii)* Vision-based solutions have higher requirements for line-of-sight and highlight [30]; *(iv)* In addition, there are some recent works provide high-precision acquisition of APs orientations based on WiFi signal, but they can only measure orientations of APs in the horizontal plane (Fig. 1a *(i)*) [24], [25].

In this paper, we propose *Anteumbler* that measures the orientations of each of WiFi APs' antennas in the physical space non-invasively, accurately and efficiently. The feasibility stems from the fact that antennas in wireless communication systems have different radiation or reception capabilities for different directions in the space. Thus, we can utilize electromagnetic wave transmission principles to correlate the received power with the spatial angle of the AP antenna.

However, there are three main challenges:

*(i)* We are unable to obtain all the antenna parameters relevant to electromagnetic wave propagation. Due to the lack of prior data on AP antennas and the inability to modify the APs, parameters such as antenna gain and polarization mismatch factor cannot be acquired. Thus, directly measuring antenna orientation based on existing models is not feasible.

*(ii)* Various factors can interfere with antenna orientation measurements. In wireless links, received power is influenced by factors such as propagation distance and environment. Since the precise environment is typically unknown in advance, determining the propagation distance of the signal in the medium and the attenuation caused by other factors becomes challenging. Consequently, directly establishing the relationship between received power and antenna orientation across all orientations is difficult.

*(iii)* To our knowledge, we are the first WiFi-based system capable of measuring the orientations of each AP antenna within physical space. Achieving this on shorter time than manual measurements (*e.g.*, minute-level) presents a challenge.

**Our solutions.** The key idea comes from the fact that there is a mapping between the electric field angles of the Tx-Rx antenna pair and the spatial angles of the local antennas (*i.e.*, the antennas used in *Anteumbler*). *(i)* Firstly, considering that received power is maximized when the local antenna and AP antenna are perfectly aligned, we construct a spatial angle model, which calculates the law of the received power with the local antenna spatial angle. This eliminates the effects of unknown antenna parameters. *(ii)* Secondly, we disambiguate the received power according to the orthogonality of antenna directivity and polarization, and construct vertical planes perpendicular to *line of sight* (LoS) paths. Specifically, we first obtain several local maxima only on these vertical planes, and then combine to obtain the global maximum to obtain the AP antenna orientation, thereby optimizing the time cost. We adopt an iterative algorithm to further improve the efficiency. *(iii)* Thirdly, we describe the AP antenna as a 3-D vector, and construct horizontal planes based on the AP antenna and its projection in the vertical plane. We use the intersection of two horizontal planes to determine the AP antenna orientation, which eliminates the influence of WiFi signal propagation distance between vertical planes. We further improve the accuracy by removing the effect of distance within the vertical plane and filtering out ambient noise.

*The main contributions of this paper are as follows:*

- We propose *Anteumbler*, to the best of our knowledge, the first attempt to measure the orientation of each antenna of AP in physical space based on WiFi signals. The advantage of *Anteumbler* is that the orientation of each antenna can be measured without prior data and without hardware/firmware modifications to APs.

- We design an optimization algorithm combining received power disambiguation with an iterative estimation process, which reduces the sampling points by hundreds of times, thus greatly improving the efficiency. We also build a dual plane intersection model to remove the influence of propagation distance, which improves the accuracy.

- We implement *Anteumbler* based on a WiFi *network interface card* (NIC) combined with a *simultaneous localization and mapping* (SLAM) robot. We test our proposed model and techniques in the real world, for different antenna types, geometries, AP heights and environments, to obtain median errors of both elevation and azimuth angles below $6\,^\circ$. Furthermore, we demonstrate the effectiveness of *Anteumbler* through case studies comparing state-of-the-art reverse localization and user localization systems.

## II. MOTIVATION

**Antenna orientation errors are common in real scenarios.** In general, the antennas of APs have four orientation errors relative to the physical space, as shown in Fig. 1a. Among them, yaw, roll and pitch show that all parallel antennas change orientations with the APs, and irregular tilt indicates that the tilt angles of the AP antennas are different. Through the investigation of 500 WiFi APs in office buildings, we found that the antennas of more than 80% APs are tilted

with angle greater than $5\,^\circ$, as shown in Fig. 1b. There are two main reasons: *(i)* In the process of deployment and use, there are inevitable manual measurement errors or external force interventions that cause the APs or antennas to tilt slightly [24]. *(ii)* To achieve higher throughput, the antennas on the APs are required to be placed in optimal positions to avoid thick concrete walls and reduce dead spots [20], [26].

**Antenna orientation errors reduce localization accuracy.** All of the above errors in antennas orientations reduce the accuracy of the localization systems based on RSSI and CSI. Specifically, according to the *Friis transmission formula* [31], the antenna tilt causes the Rx received power to change, which affects the RSSI measurement value, and then affects distance estimation result based on RSSI [18], [22], [23]. In addition, antenna orientation error also cause the separation of the array to change, which in turn affects the estimation values of AoA and ToF based on the phase of CSI [3], [24].

To verify how errors in orientations of APs or antennas affect localization accuracy, we deployed a state-of-the-art localization system in a scenario that spans $3000\,\mathrm{sq\,ft}$ in area, containing four APs equipped with three antennas. We tilt the four APs or antennas at different angles to simulate the orientation error based on the four cases in Fig. 1a, and use an algorithm similar to SpotFi [3] to locate the user's 100 different locations. From Fig. 1c, the localization error increases with the increase of the antenna orientation error, and an orientation error of $8\,^\circ$ leads to a median localization error of $1\,\mathrm{m}$. Therefore, if we locate the user based on the wrong antenna orientation, the localization accuracy is reduced.

## III. PRELIMINARIES

### A. Friis Transmission Formula

The *Friis transmission formula* [31] is used to determine the power received by a lossless and load-matched antenna in a radio communication link [32], [33]:

$$P_r = \frac{P_t G_t G_r \lambda^2}{(4\pi d)^2}, \tag{1}$$

where $P_t$, $P_r$, $G_t$ and $G_r$ are the power and gains of Tx and Rx antennas, $\lambda$ is the wavelength, $d$ is the distance between two antennas. For the application of *Friis transmission formula* to be valid, several conditions must be met [32], [33]: *(i)* $d \gg \lambda$, *i.e.*, one antenna must be in the far field of the other. *(ii)* Antennas should be properly aligned and possess identical polarization. *(iii)* Antennas must operate in free space, devoid of multipath effects. *(iv)* Directivities are assumed to be equivalent to that of isotropic radiators.

### B. Antenna Directivity and Gain

Fig. 3a depicts a point radiation source represented in spherical coordinates within free space, where the center of the sphere is the antenna phase center [32]. However, antenna usually has directivity, and its radiation space is not uniform. A power pattern is a 3-D quantity that describes power as a function of the spherical coordinates $\theta$ and $\psi$ [34], [35]. Fig. 3b depicts the radiation pattern of an omnidirectional antenna. The horizontal-plane pattern shows the uniform radiation of
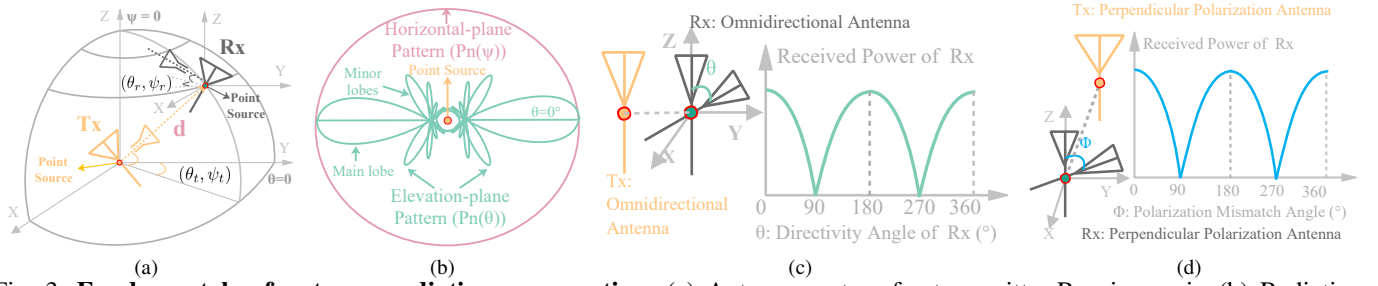
Fig. 3: **Fundamentals of antenna radiation or reception:** (a) Antenna system for transmitter-Receiver pair. (b) Radiation pattern of omnidirectional antenna. (c) Effect of directivity on received power. (d) Effect of polarization on received power.
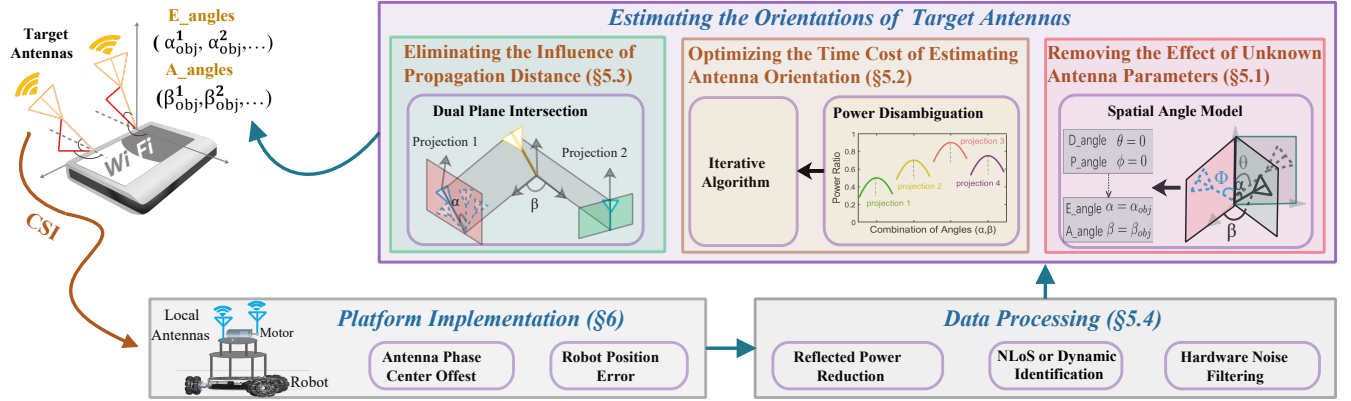


Fig. 4: **Overview: platform and implementation, data processing, estimating the orientations of target antennas.**

$360\,^\circ$. The elevation-plane pattern shows a beam with a certain width, which has the maximum radiation along the $\theta = 0\,^\circ$ direction. The antennas of WiFi APs are generally omnidirectional antennas [36]. Therefore, in this paper, we only consider omnidirectional antennas.

The directivity of antenna is the ratio of the maximum radiated power density to its average on a spherical surface in the far-field region. For an omnidirectional antenna [32]:

$$D(\theta) = \frac{4\pi}{\iint\limits_{4\pi} P_n(\theta)\mathrm{d}\Omega},\tag{2}$$

where $P_n(\theta)$ is the normalized power pattern. Fig. 3c shows the effect of antenna directivity on received power, in particular the received power is maximized when the main lobes of the two antennas are in the same direction. Antenna gain is a practical parameter, which can be expressed as [37]:

$$G(\theta) = \eta D(\theta),\tag{3}$$

where $\eta$ is the antenna efficiency related to hardware [32].

### C. Antenna Polarization Matching

Polarization serves as a crucial characteristic of antennas, delineating the trajectories of electric and magnetic field vectors as electromagnetic waves traverse space [19], [38]. When Tx and Rx antennas have the same polarization direction, the received signal is the strongest, which is polarization matching. Fig. 3d shows the effect of antenna polarization on received power, and the received power is maximized when the two antennas are parallel. For linear polarization, the polarization mismatch factor of the power is [32]:

$$F = cos^2\phi,\tag{4}$$

where $\phi$ is the difference of inclination between Tx and Rx. If the Tx is rotated in space, the received power of the Rx reduces accordingly due to polarization mismatch.

## IV. OVERVIEW

### A. Problem Statement

As shown in the left part of Fig. 4, we refer to the antennas of WiFi AP to be estimated as target antennas, and the antennas used in *Anteumbler* as local antennas. We first briefly introduce the problem of estimating target antenna's orientation in physical space, including the elevation angle (E_angle) $\alpha_{obj}^i$ and azimuth angle (A_angle) $\beta_{obj}^i$, where $i$ is the reference number of the target antennas. In our research, we assume that the location of each target antenna is known, which can be determined using a method like LocAP [24]. Note that the errors of antenna separation in LocAP increase greatly when the target antennas are tilted. But the errors have no effect on our research, because we are concerned with the true location of the target antenna (especially the antenna element). Specifically, based on the determined location of each target antenna, *Anteumbler* takes state-series WiFi signals $\mathcal{H} = \{\mathbf{H}_{\alpha_i,\beta_k} \mid \alpha_i \in [0, 2\pi), \beta_k \in [0, 2\pi)\}$ from the local antennas during several different states (combinations of E_angle and A_angle $(\alpha_i, \beta_k)$) as input, and then derives the orientations of all target antennas $(\alpha_{obj}^1, \beta_{obj}^1, \alpha_{obj}^2, \beta_{obj}^2, \cdots)$.

### B. Anteumbler Architecture

**Platform implementation & data processing.** We control *Anteumbler* to collect CSI. Then, we filter out CSI acquired under *non line of sight* (NLoS) or dynamic conditions, and leverage dual antennas to mitigate hardware noise.
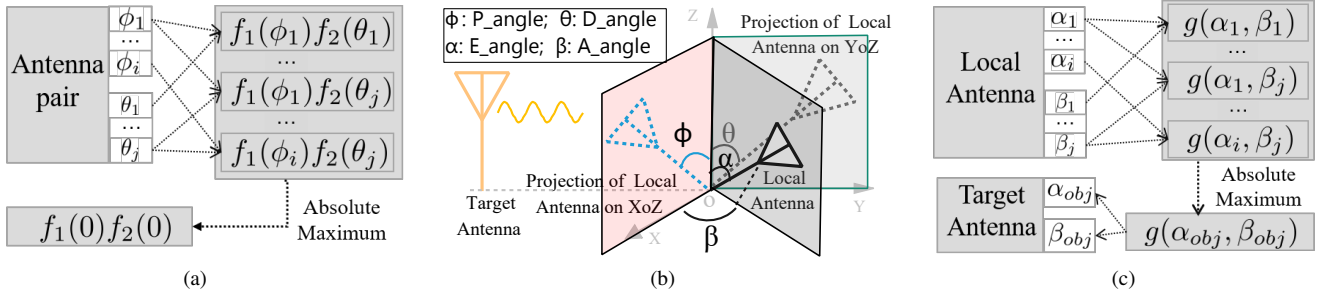
Fig. 5: **Unknown antenna parameters effect removing:** (a) For a target-local antenna pair, the received power can be expressed as the function of $\phi$ and $\theta$, and reaches the maximum when ($\phi = 0, \theta = 0$). (b) Through coordinate transformation, we convert the unknown ($\phi, \theta$) of the antenna pair to the known ($\alpha, \beta$) of the local antenna; note that ($\alpha = \alpha_{obj}, \beta = \beta_{obj}$) corresponds to ($\phi = 0, \theta = 0$). (c) For a target antenna with fixed orientation, the received power can be expressed as the function of $\alpha$ and $\beta$ of the local antenna, and reaches the maximum when ($\alpha = \alpha_{obj}, \beta = \beta_{obj}$).

**Removing the effect of unknown antenna parameters ($\phi, \theta$).** We reconstruct the *Friis transmission formula* to a spatial model, which quantifies the received power based on the known spatial angles ($\alpha, \beta$) of the local antennas.

**Optimizing the time cost of estimating antenna orientation.** We construct the vertical and horizontal planes according to the LoS path of the antenna pair, and employ an iterative algorithm within each vertical plane to enhance efficiency.

**Eliminating the influence of propagation distance.** We apply the spatial geometry principle, which asserts that the intersection of two planes is a unique line, to eliminate the impact of propagation distance.

## V. SYSTEM DESIGN

### A. Removing the Effect of Unknown Antenna Parameters

**Estimating antenna's orientation based on antenna parameters.** To estimate the orientation of the target antenna, we construct an antenna system consisting of the target antenna and the local antenna. By incorporating Equation 1 and Equation 4, and accounting for antenna directivity and polarization, we compute the received power $P_r$ of the local antenna:

$$P_r = k cos^2 \phi \cdot \frac{P_t G(\theta_t) G(\theta_r) \lambda^2}{(4\pi d)^2}, \quad (5)$$

where $k$ is the antenna efficiency factor, which is a constant, $\phi$ is the polarization mismatch angle, $P_t$ is the transmit power of the target antenna, $G_t$ and $G_r$ are the gains of target antenna and local antenna, $\lambda$ is the wavelength, and $d$ is the distance between two antennas. It is evident that changes in D_angle ($\theta_t, \theta_r$) and P_angle $\phi$ result in variations in the received power. Consequently, upon obtaining the received power $P(\phi, \theta)$, we can determine the relative angle between the target antenna and the local antenna:

$$f(\phi, \theta) = \frac{P(\phi, \theta) d^2}{P_t \lambda^2} = f_1(\phi) f_2(\theta), \quad (6)$$

where $\theta$ is the relative directivity angle between the target antenna and local antenna, which is independent of $\phi$, $f(\phi, \theta)$ is the product of two terms respectively depending on $\phi, \theta$ and reaches the absolute maximum when the two antennas are perfectly aligned (*i.e.*, $\phi = 0, \theta = 0$); see also Fig. 5a.

**Estimating antenna's orientation based on spatial angles.** Given that $\phi$ and $\theta$ are unknown, the mapping $f(\theta, \phi)$ is

unavailable. However, when the spatial angle ($\alpha_{obj}, \beta_{obj}$) of the target antenna remains constant and the spatial angle ($\alpha, \beta$) of the local antenna is known, we can convert the unknown angles ($\phi, \theta$) to the known angles ($\alpha, \beta$), as depicted in Fig. 5b. Subsequently, we can establish the mapping of the spatial angle of the local antenna to the received power:

$$g(\alpha, \beta) = \frac{P(\alpha, \beta) d^2}{P_t \lambda^2}, \alpha \in [-\frac{\pi}{2}, \frac{\pi}{2}), \beta \in [-\frac{\pi}{2}, \frac{\pi}{2}), \quad (7)$$

where $P(\alpha, \beta)$ is the received power when E_angle is $\alpha$ and A_angle is $\beta$ of the local antenna, $g(\alpha, \beta)$ is the function related to $\alpha$ and $\beta$, and reaches the absolute maximum when the two antennas are perfectly aligned (*i.e.*, $\alpha = \alpha_{obj}, \beta = \beta_{obj}$), as shown in Fig. 5c.

**Complexity analysis.** In principle, traversing the orientation of the local antenna in physical space to obtain the received power and generate a set of $g$ values is feasible. However, this approach necessitates the collection of a substantial amount of data. For instance, the time required to obtain one $g$ is $1\,\mathrm{s}$, encompassing the acceleration time of the motor, as well as the time for collecting and processing CSI. With each step angle set to $2°$, the time required for traversal becomes $(180/2)^3 = 72\,900\,\mathrm{s} = 202.5\,\mathrm{h}$, rendering it impractical. Hence, optimizing the time cost is imperative to enable the system to swiftly estimate the target antenna orientation.

### B. Optimizing Time Cost of Estimating Antenna Orientation

**Received power disambiguation.** To mitigate the time cost, we initially address the issue of ambiguity in the received power. As depicted in Fig. 6a, multiple distinct ($\alpha, \beta$) pairs may yield the same ($\phi, \theta$) values, consequently resulting in identical received power readings, leading to ambiguity. This phenomenon arises due to the correlated nature of $\alpha$ and $\beta$, as they jointly influence the received power. Noting that $\phi$ and $\theta$ are independent of each other, we can convert angles of ($\alpha \to \phi, \quad \beta \to \theta$) for received power disambiguation.

We then describe the process of antenna orientation estimation after angle conversion. As shown in Fig. 6b, we construct multiple mutually perpendicular planes based on the LoS path from the target antenna to the local antenna. We call the vertical plane ($\Pi_{\beta_1}, \Pi_{\beta_2}, \cdots$) perpendicular to the LoS path
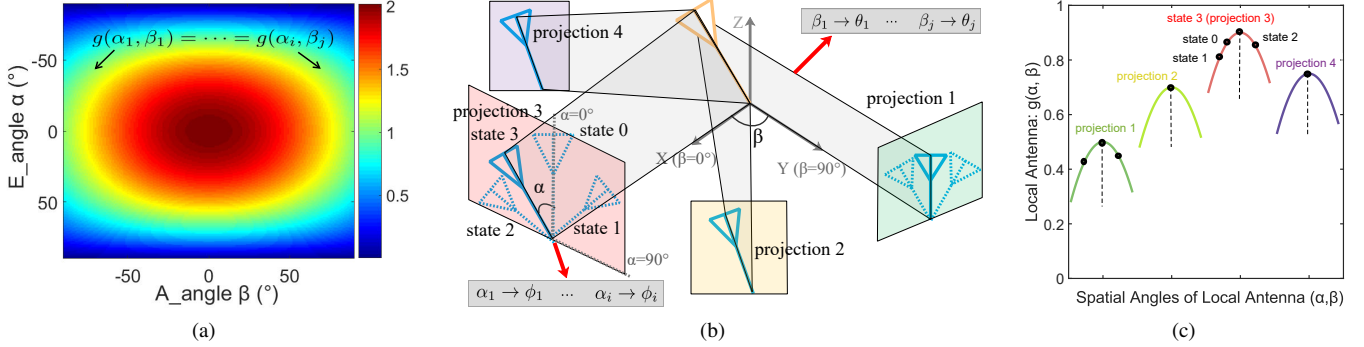
Fig. 6: **Time cost optimization and propagation distance influence removing:** (a) The local antenna exhibits same received power at different $(\alpha, \beta)$. (b) Using the orthogonality of $\phi$ and $\theta$, we convert $\alpha$ and $\beta$ to $\phi$ and $\theta$, and remove the influence of propagation distance based on the geometric principle of plane intersection. (c) The orientation of the target antenna can be quickly obtained by solving for the relative maximum of each vertical plane and then for their absolute maximum.

and the horizontal plane $(\Pi_1, \Pi_2, \cdots)$ parallel to the LoS path. First, we rotate the local antenna in one certain vertical plane $\Pi_{\beta_k}$, and the E_angle is $\alpha$. This process is carried with fixed $(\theta = \theta_k)$, thus the function $g$ is only related to $\phi$ ($\alpha \to \phi$). Hence, in plane $\Pi_{\beta_k}$, we obtain:

$$g_{1_k}(\alpha) = g(\alpha, \beta)|_{\beta=\beta_k} = \frac{P(\alpha)d^2}{f_2|_{\theta=\theta_k}P_t\lambda^2}, \ \ k \in [1, K], \quad (8)$$

where K is the number of vertical planes. As shown in Fig. 6c, we get a E_angle $\alpha_{\beta_k}$ corresponding to the relative maximum of $g_{1_k}(\alpha)$ in plane $\Pi_{\beta_k}$:

$$\alpha_{\beta_k} = \arg\max_{\alpha} \ g_{1_k}(\alpha), \quad (9)$$

where $g_{1_k}(\alpha)$ reaches the relative maximum only when $\phi = 0$, and $\alpha = \alpha_{\beta_k}$ at this time. Second, for the relative maximum of each vertical plane, we fix $\phi$ ($\phi = 0$), so the function $g$ is only related to $\theta$ ($\beta \to \theta$). Hence, in plane $\Pi_k$, we can obtain the following:

$$g_{2_k}(\beta) = g(\alpha, \beta)|_{\alpha=\alpha_{\beta_k}} = \frac{P(\beta)d^2}{f_1|_{\phi=0}P_t\lambda^2}, \ \ k \in [1, K]. \quad (10)$$

As shown in Fig. 6c, we can measure an absolute maximum of $g_{2_k}(\beta)$ in planes $\Pi_k$ and get the angle:

$$\beta_{obj} = \arg\max_{\beta} \ g_{2_k}(\beta), \quad (11)$$

where $g_{2_k}(\beta)$ reaches the absolute maximum only when $\theta = 0$, and $\alpha = \alpha_{obj}, \beta = \beta_{obj}$ at this time. Obviously, the $g(\alpha_{obj}, \beta_{obj})$ is the absolute maximum in different horizontal planes, and is also the absolute maximum in different vertical planes. Therefore, the angle combination $(\alpha_{obj}, \beta_{obj})$ is the orientation of the target antenna in physical space.

**Iterative algorithm.** Naively, we can measure $g$ over the range $[-\pi/2, \pi/2]$ of $(\alpha, \beta)$, but the time cost is still huge. For example, traversing the range of $\alpha$ in each vertical plane, and assuming that the time cost to obtain one $g$ is $1\,\text{s}$, the steps of $\alpha$ and $\beta$ are $2°$, then the time cost is $(180/2+1)^2 = 8281\,\text{s} \approx 138\,\text{min}$. To further optimize the time cost, we aim to reduce the number of vertical planes and measurements within each vertical plane. The key insight is that the closer the vertical plane is to perfect alignment, the greater the projection's E_angle, as depicted in Fig.6b. Consequently, we can swiftly estimate $\alpha_{obj}$ and $\beta_{obj}$ in an iterative fashion. Initially, we execute the procedure outlined in Equations8-11 within only

two adjacent vertical planes to discern the orientation trend of the target antenna (average time cost: $((180/2)/2)\times 2 = 90\,\text{s}$). Subsequently, we adjust the position and orientation of the local antenna towards this trend based on the previous vertical plane's state, until the absolute maximum is reached (average time: $(180/2)/2 = 45\,\text{s}$). The total time cost is $135\,\text{s}$. However, the iterative algorithm heavily relies on measurements from the previous state. Errors in $g$ can significantly impact the accuracy of the target antenna orientation. Therefore, we need to mitigate factors that influence $g$, such as propagation distance $d$ and ambient noise.

### C. Eliminating the Influence of Propagation Distance

To remove the influence of propagation distance on $g$, our primary approach is to ensure that measurements in each vertical plane are independent. An important observation is that the projection of the target antenna in each vertical plane corresponds to the relative maximum of $g$ within that plane, as shown in Fig. 6b. Then, we can obtain the target antenna orientation by utilizing two independent vertical planes based on the spatial geometry principle of "*intersection of two intersecting planes*". The specific solution is given below.

In the following, both the target antenna and the local antenna are described as 3-D vectors. The unit direction vector of the target antenna is defined as:

$$\hat{\mathbf{e}}_{\mathbf{d}} = (\sin\hat{\alpha}_{obj}^m \cos\hat{\beta}_{obj}^m, \sin\hat{\alpha}_{obj}^m \sin\hat{\beta}_{obj}^m, \cos\hat{\alpha}_{obj}^m), \quad (12)$$

where $m \in [1, \cdots, M]$ and $M$ is the number of target antennas. The unit normal vector of vertical plane $\Pi_{\beta_k}$ at $\beta_k$:

$$\mathbf{e}_{\mathbf{n}_{\beta_k}} = (\cos\beta_k, \sin\beta_k, 0), \quad for \quad k = 1, 2, \cdots, K. \quad (13)$$

In plane $\Pi_{\beta_k}$, the E_angle is $\hat{\alpha}_{\beta_k}^m$ when $P$ reaches its relative maximum, and the local antenna is the projection of the target antenna in the vertical plane, so the unit direction vector of projection is:

$$\hat{\mathbf{e}}_{\mathbf{d}_{\beta_k}} = (-\sin\hat{\alpha}_{\beta_k}^m \sin\beta_k, \sin\hat{\alpha}_{\beta_k}^m \cos\beta_k, \cos\hat{\alpha}_{\beta_k}^m). \quad (14)$$

Thus, the unit normal vector of the plane $\Pi_k$ constructed by the target antenna and its projection:

$$\hat{\mathbf{e}}_{\mathbf{n}_k} = \hat{\mathbf{e}}_{\mathbf{d}_{\beta_k}} \times \mathbf{e}_{\mathbf{n}_{\beta_k}}$$
$$= (\cos\hat{\alpha}_{\beta_k}^m \sin\beta_k, -\cos\hat{\alpha}_{\beta_k}^m \cos\beta_k, \sin\hat{\alpha}_{\beta_k}^m). \quad (15)$$

This article has been accepted for publication in IEEE Transactions on Mobile Computing. This is the author's version which has not been fully edited and content may change prior to final publication. Citation information: DOI 10.1109/TMC.2024.3485228
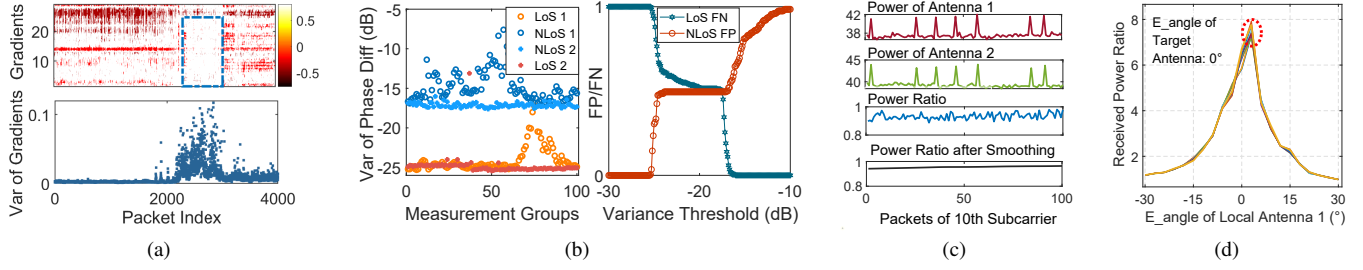
7



Fig. 7: **Data processing:** (a) Dynamic packets can be identified by the variance of subcarriers' gradient. (b) NLoS identification based on dual antenna phase difference variance. (c) Received power ratio after filtering hardware noise by dual antenna ratio and data smoothing. (d) We estimate the E_angle of target antenna based on the extracted received power ratio.

---

**Algorithm 1** Estimating Target Antennas' Orientations.

---

**Input:** Power of Local Antennas at state $\alpha_i$ of position $\beta_k$: $\mathbf{P} = \{P^1_{(\alpha_0,\beta_0)}, \cdots, P^M_{(\alpha_0,\beta_0)}\}, \cdots, \{P^1_{(\alpha_i,\beta_k)}, \cdots, P^M_{(\alpha_i,\beta_k)}\}, \cdots\}$, the number of position K, the number of target antennas M.

**Output:** Target antennas orientations: $(\hat{\alpha}^1_{obj}, \hat{\beta}^1_{obj}, \cdots, \hat{\alpha}^M_{obj}, \hat{\beta}^M_{obj})$.

1: **for** $k \leftarrow 1; k <= K; k++$ **do**
2:     flag_forward = zeros(M);
3:     flag_backward = zeros(M);
4:     $i \leftarrow 0$;
5:     **while** $notall(flag\_backrward) == 1$ **do**
6:         Motor rotates clockwise, $i \leftarrow i + 1$;
7:         **if** $P^m_{(\alpha_i,\beta_k)} < P^m_{(\alpha_{i-1},\beta_k)}$ **then**
8:             flag_backward(m-1) = 1;
9:         **end if**
10:     **end while**
11:     **while** $notall(flag\_forward) == 1$ **do**
12:         Motor rotates counterclockwise, $i \leftarrow i + 1$;
13:         **if** $P^m_{(\alpha_i,\beta_k)} < P^m_{(\alpha_{i-1},\beta_k)}$ and $P^m_{(\alpha_{i-2},\beta_k)} < P^m_{(\alpha_{i-1},\beta_k)}$
    **then**
14:             $\hat{\alpha}^m_{\beta_k} \leftarrow \alpha_{i-1}$;
15:             flag_forward(m-1) = 1;
16:         **end if**
17:     **end while**
18: **end for**
19: **for** $m \leftarrow 1; m <= M; m++$ **do**
20:     $(\hat{\alpha}^m_{obj}, \hat{\beta}^m_{obj}) \leftarrow Equation\ 16$;
21:     **return** $(\hat{\alpha}^m_{obj}, \hat{\beta}^m_{obj})$.
22: **end for**

---

In theory, $\hat{\mathbf{e}}_\mathbf{d}$ should always be perpendicular to $\hat{\mathbf{e}}_{\mathbf{n_k}}$:

$$\hat{\mathbf{e}}_\mathbf{d} \cdot \hat{\mathbf{e}}_{\mathbf{n_k}} = 0, \quad for \quad k = 1, 2, \cdots, K. \tag{16}$$

Next, we estimate the E_angle $\hat{\alpha}^m_{obj}$ and the A_angle $\hat{\beta}^m_{obj}$ based on measurements from two distinct vertical planes. Furthermore, we employ an iterative algorithm to swiftly determine the relative maximum $\hat{\alpha}^m_{\beta_k}$ within each vertical plane, with an average time cost of $(180/2/2) \times 2 = 90\,\text{s}$. Finally, we leverage multiple vertical planes to address the least squares problem and enhance accuracy. The process of estimating the target antenna orientation is given in Algorithm 1. Additionally, while the propagation distance undergoes slight changes as the local antenna rotates within each vertical plane, these alterations are minor and are analyzed in Section VI-B.

### D. Data Processing

**Reflected power reduction.** Up to this point, we have assumed the existence of only one LoS path from the WiFi AP to the robot. However, the presence of multipath in
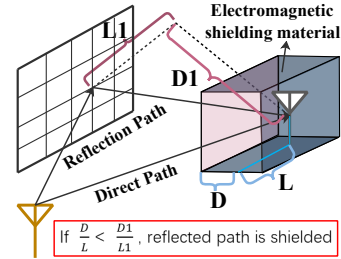


Fig. 8: **We add electromagnetic shielding material around the local antennas to reduce the reflected power since the direction of the direct path is known.**

the environment can introduce significant inaccuracies to our algorithms due to distortions in power measurements. Our observation is that the LoS path is known in our problem as mentioned in Section IV-A, so we can mitigate the power of multipath reflections through hardware measures. Specifically, we have incorporated materials around the local antennas that are readily available and effectively shield electromagnetic wave signals [39]. The reflected signal is shielded when the propagation path meets the condition: $\frac{D}{L} < \frac{D_i}{L_i}$, where $D$ and $L$ are the dimensions of the electromagnetic shielding box, $D_i$ and $L_i$ are the distance components of the $i$-th reflection path to the electromagnetic shielding box in two vertical directions, as shown in Fig. 8.

**Dynamic environment identification.** The dynamic external environment also affects the measurement of CSI, thereby affecting the estimation accuracy of the antenna orientation. We use the variation of the phase gradient between subcarriers to identify the dynamic environment, similar to the method in [40]. As shown in Fig. 7a, the gradient variance of the static environment should be smaller. Next, we directly remove the CSI of the dynamic environment.

**NLoS identification.** Another critical factor to consider is the presence of NLoS, especially when the local antenna rotates within the same vertical plane, the simultaneous presence of LoS and NLoS situations can result in significant power fluctuations [41], [42], making accurate measurement of the projection challenging. To address this, we employ a method similar to PhaseU [43] to identify LoS/NLoS conditions. Specifically, NLoS conditions involve more abundant reflections, diffractions, and refractions, leading to signals traveling through NLoS paths behaving more randomly in terms of amplitude and phase [43]. We quantify the difference between LoS and NLoS by incorporating the frequency diversity feature
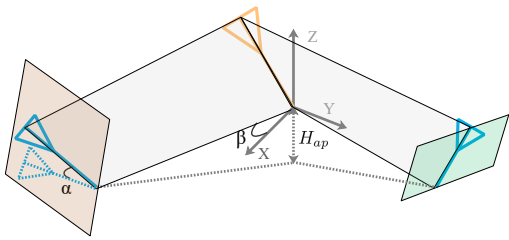
Fig. 9: **Generalizing to 3D:** $H_{ap}$ **is the vertical height from target antenna to local antenna, where the vertical planes are inclined to the ground but perpendicular to LoS.**

as a weight parameter to compute the spatial phase difference variance of the two antennas. As shown in Fig. 7b, LoS/NLoS can be distinguished based on a certain threshold. To create NLoS conditions, we utilize two different types of obstacles that are relatively common in the real-world (concrete pillar and wooden board). Specifically, we set the threshold at -20dB (based on empirical values from our test environment), and consider it as NLoS when the variance exceeds the threshold. Subsequently, we optimize the algorithm: if NLoS is identified, the target antenna is not measured at this position, and we proceed to the next position instead.

**Hardware noise filtering.** We employ an *industrial personal computer* (IPC) equipped with NIC to collect CSI. However, the accuracy of CSI estimation is influenced by hardware noise, including uncertainties in power control due to *automatic gain control* (AGC) and electromagnetic noise [44]. In the case of *multi-input multi-output* (MIMO) systems, the noise levels across multiple antennas at the same sample tend to be similar, enabling the utilization of the dual antenna ratio for filtering hardware noise [45]. As depicted in Fig.7c, the power ratio exhibits greater stability compared to using a single antenna. Subsequently, we extract stable received power based on the CSI processed through the aforementioned methods, as shown in Fig.7d, which effectively facilitates accurate measurement of the E_angle of the target antenna.

It is worth noting that the data packet rate of commercial WiFi devices may be relatively low, so we provide a specific analysis here. In data processing, dynamic environment identification filters out any packets with significant fluctuations, and NLoS identification can be completed across the entire vertical plane. The dual-antenna ratio method is also independent of the data rate. Therefore, in *Anteumbler*, we can consider that the CSI data packet rate does not significantly impact our measurement accuracy.

### E. Generalizing to Three Dimensions

*Anteumbler* can be generalized to 3-D. This generalization is important, because APs are usually located above ground, around $2\,\text{m}$ in real-world deployments. To better understand our solution, consider a situation where the target antenna is above the vertical height $H_{ap}$ from the local antenna, as shown in Fig. 9. We can construct *Anteumbler* based on the vertical planes, where the vertical planes are not perpendicular to the ground, and the tilt angle is: $\Theta = \arctan\frac{H_{ap}}{d_{ap}}$, $d_{ap}$ is the horizontal distance from the local antenna to the target antenna. We convert 3-D to 2-D, and get the orientations of the target antennas using Equation 9 and Equation 16.
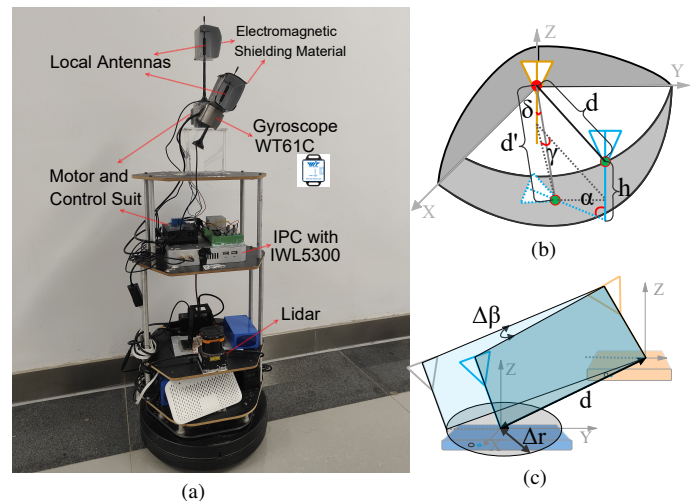


Fig. 10: **Platform:** (a) *Anteumbler*. (b) Phase center offset of local antenna due to rotation ($\gamma$ in the horizontal plane, $\pi/2-\delta$ in the vertical plane, and $d'-d$ in distance). (c) Effects of bot's position error ($\Delta r \to \Delta\beta$).

## VI. PLATFORM IMPLEMENTATION

### A. Anteumbler Implementation

As shown in Fig. 10a, we build *Anteumbler* based on an IPC with WiFi NIC IWL5300, and with Intel Core i7-5550U CPU and $4\,\text{GB}$ RAM, running on Ubuntu 14.04 LTS. We install *Linux 802.11 CSI Tool* on the IPC and keep it in communication with the target WiFi APs to collect CSI [46]. The local antennas are perpendicular polarized omnidirectional dipole antennas with an element length of $4\,\text{cm}$. We use a two-phase stepper motor UMot 57HS5417-21-500U [47] with a motion control suit and a two-way relay to control the rotation of local antenna 1. We add electromagnetic shielding material [48] around the local antennas to shield most of the reflected path signal. We fix a high-precision gyroscope WT61C [49] at the center of the local antenna 1 to measure this antenna's angles in physical space.

Then, in order to automatically measure the antennas' orientations of WiFi APs, we mount the above system on the TurtleBot platform [50], a low-cost open-source robotics development kit. We mount the Hokuyo UTM-30LN LI-DAR [51] to capture most obstacles in the environment. We place the local antennas on the top of TurtleBot to have the widest field of view. TurtleBot is controlled via the Robot Operating System (ROS Kinetic), giving us access to a number of software packages for SLAM and navigation. We choose Gmapping [52] as the SLAM algorithm to construct the physical map, and make TurtleBot autonomously navigate to several target points around the target AP. Next, before evaluating *Anteumbler*, we need to determine how the local antennas and robot affect our system.

### B. Phase Center Offset of Local Antennas

The antenna phase center is an equivalent parameter, and is the actual reference point of receiving or transmitting [53], [54]. In this paper, the local antenna is dipole antenna whose phase center is in the plane of its main lobe [32]. In theory, we

This article has been accepted for publication in IEEE Transactions on Mobile Computing. This is the author's version which has not been fully edited and content may change prior to final publication. Citation information: DOI 10.1109/TMC.2024.3485228
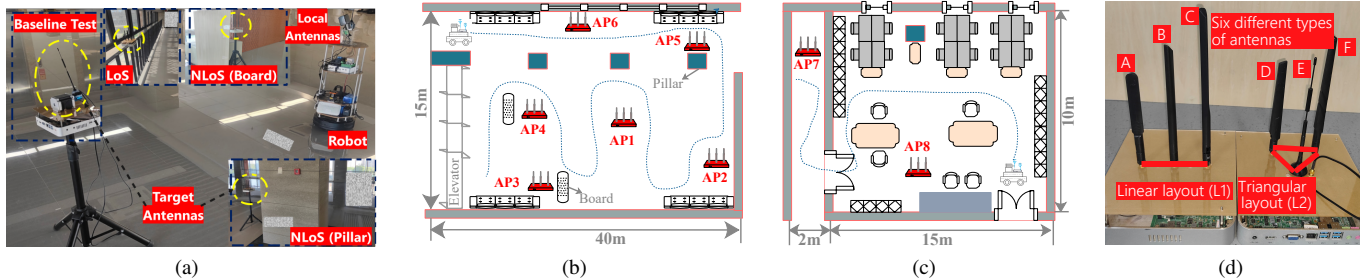
9

Fig. 11: **Experimental setup:** (a) Experimental deployment. (b) Hall: A weak-multipath-level scenario. (c) Office: A strong-multipath-level scenario. (d) Six different types of antennas and two different antenna layouts.

can use the geometric position corresponding to the maximum gain direction of the local antenna as the rotation point to make it rotate within the vertical plane. In practice, however, we cannot accurately fix the rotation point in the direction of maximum gain of the local antenna 1, so the phase center varies within the vertical plane. As shown in Fig. 10b, $h$ is the height from the real phase center to the rotation point, and $d$ is the propagation distance from the target antenna to the local antenna. When the antenna rotates by $\alpha$, the propagation distance from the target antenna to the local antenna is $d'$, and $\gamma$ and $\delta$ are the drift angle in the horizontal plane and the complement of the drift angle in the vertical plane respectively. According to their geometric relationship, the following equations are established:

$$\begin{cases} h - h\cos\alpha = d'\cos\delta \\ h\sin\alpha = d\tan\gamma \\ d'\sin\delta = d\sec\gamma. \end{cases} \quad (17)$$

Then, we solve the system of equations:

$$\begin{cases} \gamma = \arctan\dfrac{h\sin\alpha}{d} \\ \delta = \arctan\dfrac{\sqrt{h^2\sin^2\alpha + d^2}}{h(1-\cos\alpha)} \\ d' = \sqrt{2h^2(1-\cos\alpha) + d^2}. \end{cases} \quad (18)$$

For an omnidirectional antenna, the offset angle $\gamma$ of the local antenna 1 in the horizontal plane is the same. When the height from the rotation point to the phase center $h < 5\,\mathrm{cm}$ and the propagation distance $d > 3\,\mathrm{m}$, then $\delta > 89°$ and $d' - d < 0.13\,\mathrm{cm}$. We fix the rotation point of the local antenna 1 at a position less than $5\,\mathrm{cm}$ below the center of the antenna, so that the influence of the phase center offset can be ignored. *Note that both $h$ and $d$ in Equation 18 can be flexibly replaced.*

### C. Effects of Bot's Position Error

We use Gmapping as the SLAM algorithm and navigate the robot, so it is necessary to analyze the impact of navigation errors on *Anteumbler*. In our antenna orientation estimation algorithm, the dual-plane intersection model operates independently of the propagation distance. Therefore, the issue related to the SLAM navigation that might affect *Anteumbler*'s accuracy is the position error of the robot itself. We first test the reported position error of the robot, and we can obtain that the median error $\Delta r$ is around $10\,\mathrm{cm}$. *Anteumbler* requires that the local antenna 1 rotate within the plane

perpendicular to LoS. Therefore, the error of robot position is represented by the mapping of the target antenna to another plane: $\beta_k \rightarrow (\beta_k + \Delta\beta_k)$, as shown in Fig. 10c, the error of this A_angle is $\Delta\beta_k$. When the propagation distance $d > 3\,\mathrm{m}$, we can get $\Delta\beta < \arctan\frac{0.1}{3} \approx 1.9°$, so the effects on $\Delta\beta_k$ can be neglected in Equation 15. As for the orientation of the robot, we use the high-precision gyroscope WT61C to correct it, so the orientation error can also be ignored.

## VII. EVALUATION

### A. Experimental Setup

We evaluate *Anteumbler*'s performance in two real-world environments. The first scenario is a hall with weak multipath effects, spanning $6500\,\mathrm{sq\,ft}$, as shown in Fig.11a and Fig.11b. In the hall, we deploy six APs, covering both LoS and NLoS conditions (with obstacles such as pillars and boards). The second scenario is an office with strong multipath effects, covering an area of $1800\,\mathrm{sq\,ft}$, as shown in Fig.11c. In the office, we place two APs to capture varying multipath information. Across these eight AP locations, depicted in Fig.11d, we test two antenna geometries (linear and triangular layouts) and six different antenna types (all perpendicularly polarized omnidirectional antennas). Additionally, we vary the AP heights to evaluate the 3-D effects, as shown in Fig. 15a. We use a high-precision gyroscope WT61C as the ground truth for the orientations of the target antennas. It is worth noting that although we use test scenarios with areas different from those in Section I, it still meets our requirement of achieving less than 1 m of localization error in an area equivalent to $3000\,\mathrm{sq\,ft}$, as the average area of these two scenarios is greater than $3000\,\mathrm{sq\,ft}$.

### B. Microscopic Benchmark

**Baseline accuracy of E_angle.** To verify the baseline accuracy of E_angle, we fix one target antenna on a stepper motor and rotate it to $0°$, $20°$, $45°$, $70°$, $90°$ (*i.e.*, $\alpha_{obj}$) as depicted in Fig. 11a, and then estimate them. We place robot in LoS condition and rotate the local antenna 1 from $-90°$ to $90°$ (*i.e.* $\alpha_i$) with a step length of $2°$ for a total of 90 states. In each state, we collect one second CSI to calculate the received power ratio, and repeat this process 100 times. Note that the target antenna is parallel to the rotation plane of the local antenna, *i.e.*, the A_angle of the local antenna and the target antenna are always consistent (*i.e.*, $\beta_{obj} = \beta_k$). Considering that APs are placed in different locations resulting in different
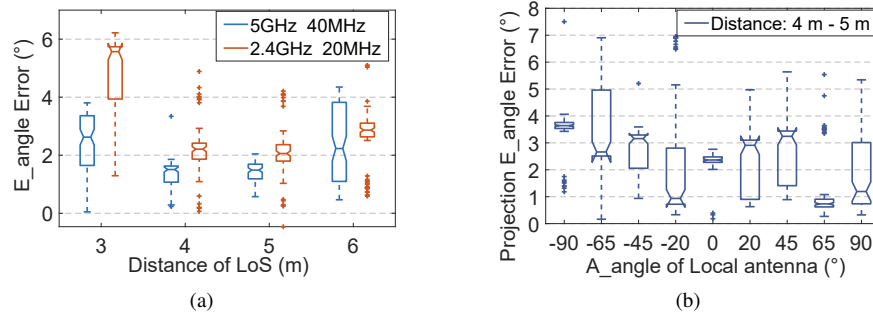
Fig. 12: **Baseline accuracy:** (a) Accuracy of E_angle for different bands and propagation distances. (b) Accuracy of projection E_angle for different A_angle.
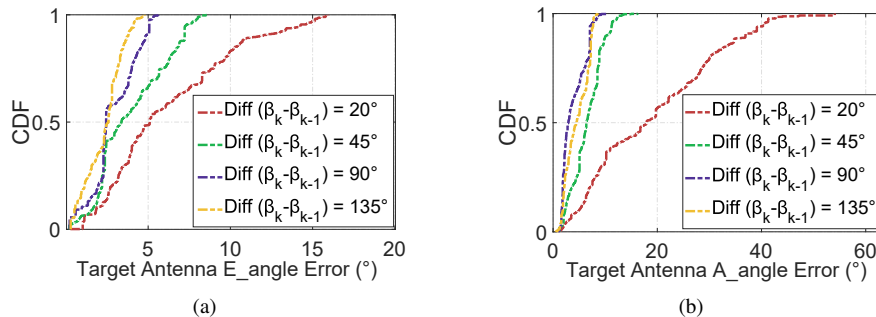


Fig. 13: **Orientation accuracy of target antenna:** (a) Estimation accuracy of E_angle. (b) Estimation accuracy of A_angle.
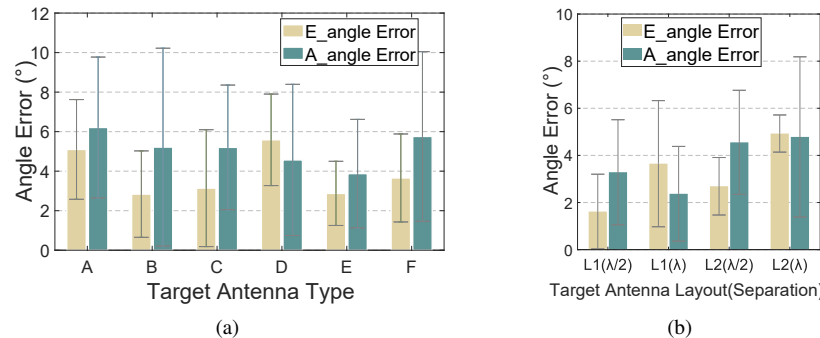


Fig. 14: **Impact of target antenna types and layouts:** (a) Accuracy for six different antenna types. (b) Accuracy for two different antenna layouts (L1: triangular layout, L2: linear layout) and two different antenna separations ($\lambda/2$ and $\lambda$).

LoS propagation distances. To mimic this, we set the LoS distances to $3\,\text{m}$, $4\,\text{m}$, $5\,\text{m}$, $6\,\text{m}$ and collect CSI to estimate E_angle. Further, APs usually operate at $2.4\,\text{GHz}$ or $5\,\text{GHz}$ bands with $20\,\text{MHz}$ or $40\,\text{MHz}$ bandwidth, so we collect CSI with the same setup for $5\,\text{GHz}/40\,\text{MHz}$ and $2.4\,\text{GHz}/20\,\text{MHz}$. The baseline accuracy of E_angle is shown in Fig. 12a, and the E_angle errors under all conditions are below $6\,^\circ$. Among them, the accuracy of the LoS distance $4\,\text{m}$ and $5\,\text{m}$ is better than that of $3\,\text{m}$ and $6\,\text{m}$. This is due to platform implementation. Specifically, the phase center offset of local antenna and the error of robot are larger when the distance is short, and the multipath effect increases when the distance is long. Hence, in order to obtain better accuracy, we control the LoS distance to the optimal $4\,\text{m}$-$5\,\text{m}$. In addition, the accuracy of $5\,\text{GHz}/40\,\text{MHz}$ is better than that of $2.4\,\text{GHz}/20\,\text{MHz}$, which is caused by the different influence of CSI noise.

**Effect of A_angle on projection E_angle.** Since we rotate the local antenna 1 in different vertical planes and obtain the E_angle of its projection in each vertical plane, we need to verify the accuracy of the projection E_angle in different vertical planes, *i.e.*, the effect of A_angle on projection E_angle. We fix one target antenna on a stepper motor and rotate it to $10\,^\circ$, $30\,^\circ$, $60\,^\circ$ (*i.e.* $\alpha_{obj}$) and A_angle is fixed to $90\,^\circ$ (*i.e.* $\beta_{obj}$). Then we collect CSI by rotating the local antenna 1 in the vertical planes with A_angle of $-90\,^\circ$, $-65\,^\circ$, $-45\,^\circ$, $-20\,^\circ$, $0\,^\circ$, $20\,^\circ$, $45\,^\circ$, $65\,^\circ$, $90\,^\circ$ (*i.e.* $\beta_k$) and calculate the projection E_angle respectively, and we repeat this process 100 times. We use Equation 16 in combination with $\sin^2 \hat{\alpha}_{\beta_k} + \cos^2 \hat{\alpha}_{\beta_k} = 1$ to calculate the ground truth of the projection E_angle. As shown in Fig. 12b, the projection E_angle errors are below $6\,^\circ$ for different vertical planes.

**Physical orientation accuracy of target antenna.** Based on the above two baseline tests, we estimate the physical orientation of the target antenna in the hall scenario. We set the three antennas on each WiFi AP to different orientations, for example, AP1 = $\{(30\,^\circ, 0\,^\circ), (45\,^\circ, 0\,^\circ), (45\,^\circ, 0\,^\circ)\}$, and AP2 = $\{(0\,^\circ, 0\,^\circ), (45\,^\circ, 0\,^\circ), (30\,^\circ, -90\,^\circ)\}$. For each AP, we rotate the local antenna 1 with a step length of $2\,^\circ$ in the vertical planes around it to collect CSI, where A_angle of the vertical planes are $-90\,^\circ$, $-65\,^\circ$, $-45\,^\circ$, $-20\,^\circ$, $0\,^\circ$, $20\,^\circ$, $45\,^\circ$,
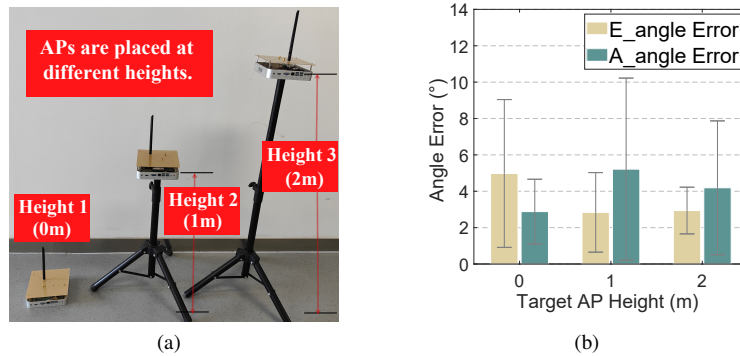
(a)



(b)

Fig. 15: **Impact of target AP heights:** (a) Three different AP heights. (b) Accuracy of angles for three different AP heights.



(a)



(b)



(c)



(d)

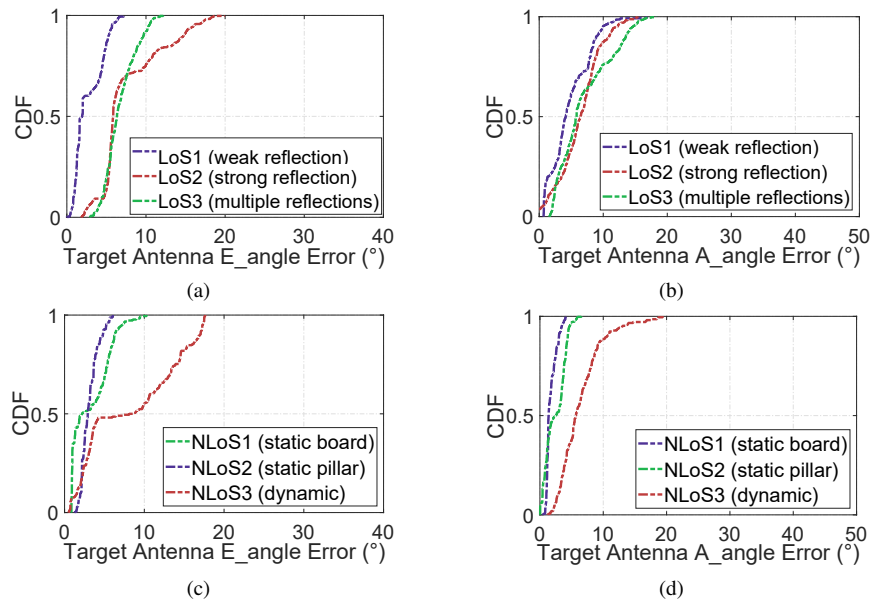Fig. 16: **Impact of environments:** (a) Accuracy of E_angle and (b) Accuracy of A_angle in three different LoS scenarios. (c) Accuracy of E_angle and (d) Accuracy of A_angle in three different NLoS scenarios.

$65\,^{\circ}$, $90\,^{\circ}$ (*i.e.* $\beta_k$). We then estimate the physical orientations of the target antennas based on some two vertical planes combined with least squares, and the results are shown in Fig. 13a and Fig. 13b. We further compare the estimation accuracy using two vertical planes with different spacing (*i.e.* Diff($\beta_k - \beta_{k-1}$)). It can be seen from Fig. 13a and Fig. 13b that as the spacing of the vertical planes increases, the estimation error decreases, and the best accuracy is achieved when the spacing is $90\,^{\circ}$. At this time, the median error of E_angle is $3\,^{\circ}$, and the median error of A_angle is $4\,^{\circ}$. The reason for this is that when the vertical plane spacing is $90\,^{\circ}$, the effect between them is minimal. Therefore, we propose to use two vertical planes spaced by $90\,^{\circ}$ to estimate the physical orientation of the antenna. Of course, when some narrow areas cannot meet $90\,^{\circ}$, the spacing can be reduced.

### C. Macroscopic Benchmark

**Impact of antenna types.** APs may be equipped with different antennas, and different types of antennas have different power lobe patterns, resulting in different power attenuations. We test six different types of antennas in the hall scenario as shown in Fig. 11d. The heights of these six antennas are different, and the lengths of the antenna elements are also

different. The test results are shown in Fig. 14a, it can be seen that for different types of antennas, the median errors of E_angle are below $6\,^{\circ}$, and the median errors of A_angle are also below $6\,^{\circ}$. In addition, the estimation accuracy of different types of antennas is different because the antenna element itself is slightly bent or tilted.

**Impact of antenna layouts.** There are two common geometric layouts of APs, linear and triangular, as shown in Fig. 11d, and the spacing between antennas is different. We test two antenna layouts in the hall scenario using one type of antenna, and the antenna spacing is set to $\lambda/2$ and $\lambda$, a total of four combinations. As shown in Fig. 14b, the median errors of both E_angle and A_angle are below $6\,^{\circ}$. Among them, L1 is triangular layout, L2 is linear layout. The reason why the accuracy of triangular layouts is better than that of linear layouts is that our system uses the center of the antenna combination as the reference point to construct LoS paths, and the deviation of triangular layouts is smaller than that of linear layouts, which can also be seen from the increase in the estimation error as the antenna spacing increases.

**Impact of AP heights.** APs may be placed at different heights. In order to verify the performance of *Anteumbler* in 3-D, we test three antenna orientations with different AP heights

This article has been accepted for publication in IEEE Transactions on Mobile Computing. This is the author's version which has not been fully edited and content may change prior to final publication. Citation information: DOI 10.1109/TMC.2024.3485228
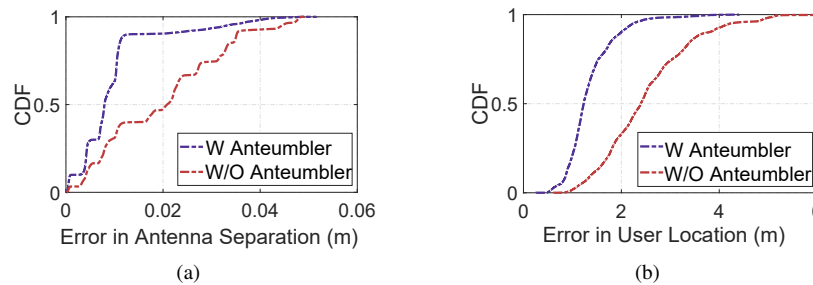
12



Fig. 17: **Case studies when APs or antennas are tilted:** (a) Antenna separation accuracy in reverse localization with or without *Anteumbler*. (b) User localization accuracy with or without *Anteumbler*.

(*i.e.*, $0\,\mathrm{m}$, $1\,\mathrm{m}$, $2\,\mathrm{m}$) in the hall scenario, as shown in Fig. 15a. The test results is shown in Fig. 15b, it can be seen that for different AP heights, the median errors of E_angle and A_angle are all below $6\,^{\circ}$.

**Impact of environments.** We test *Anteumbler*'s ability in different environments. First, the condition of AP7 is to have one or two strong reflections, and the condition of AP8 is to have multiple reflections. The results are then compared with the weakly reflected conditions in the hall scenario. As shown in Fig. 16a and Fig. 16b, the accuracy is reduced in complex multipath, but the median errors are all below $6\,^{\circ}$. Second, we test in different NLoS, static pillar and wooden, and dynamic NLoS (people moving with objects). As shown in Fig. 16c and Fig. 16d, under static NLoS, although there is power attenuation, the attenuation trend is the same, so it has better accuracy. However, under dynamic NLoS, the trend of attenuation is different, so the accuracy decreases, but the median errors are below $6\,^{\circ}$.

### D. Case Studies

We deploy LocAP and SpotFi, state-of-the-art reverse localization and user localization systems, in the hall scenario to validate the effect of *Anteumbler*. We place four APs at different positions in the hall and make the APs or antennas tilted irregularly. We use a laser rangefinder [55] and a WT61C to determine the ground truth of antennas and user.

**Case study 1: reverse localization.** We first deploy LocAP. We set the antenna separation as $\lambda$ and fix the orientation of these APs. Then we move the robot along a straight line, collect one set of CSI every $5\,^{\circ}$, a total of 20 sets for estimating the antenna separation, and repeat this process 100 times. Next, we deploy *Anteumbler* to estimate the physical orientation of these antennas and correct them. After that, the antenna separation is estimated with the same setup. The result is shown in Fig. 17a. Obviously, when the antennas are tilted irregularly, the error of the antenna separation by LocAP is greatly increased. After the antennas orientations are corrected by *Anteumbler*, the error is reduced by $10\,\mathrm{mm}$.

**Case study 2: user localization.** Finally, we deploy SpotFi. We set the antenna separation as $\lambda/2$ to obtain the best localization effect. A user with a smartphone connects to these four APs and moves to 40 different locations. We collect CSI and use them to calculate user's location. Next, we deploy *Anteumbler* to estimate the physical orientation of these antennas and artificially correct them. After that, the

user's location is estimated with the same setup. As shown in Fig. 17b, the error of user location by SpotFi increases when the antennas are tilted irregularly. After the antennas orientations are corrected by *Anteumbler*, the error is reduced by more than $1\,\mathrm{m}$.

## VIII. Discussions

**Non-linearly polarized antenna.** *Anteumbler* currently considers linearly polarized antennas. In addition, many researches have been devoted to circularly polarized or elliptically polarized antennas for localization and sensing [14]–[16]. For elliptically polarized antennas, the electric field has components in two directions that are perpendicular to each other and there is a phase difference between the components [32]. We can estimate the antenna orientation by measuring the long axis direction based on the same method of *Anteumbler*. Note that the larger the ratio of the major axis to the minor axis, the higher the estimation accuracy. For circularly polarized antennas, where the electric field components are the same, our model no longer applies. Fortunately, circularly polarized antennas have no polarization mismatch.

**AP with a large number of inside antennas.** For antennas embedded inside AP, *Anteumbler* is still a good choice, since the overall tilt of the APs also exists, as described in Section 1 and Section 2. Furthermore, it is true that APs with a large number of antennas or densely deployed can significantly improve localization accuracy. However, we still hope that *Anteumbler* can serve WiFi-based sensing scenarios that do not have these deployments or require extremely high accuracy (*e.g.*, WiFi-based imaging and material identification), not just ordinary localization systems.

**SLAM Robot and motor platform.** It should be emphasized that although we build *Anteumbler* based on the SLAM robot to work, the design does not depend on it. Our purpose of using robot and motor is to let us collect the required test samples automatically, thus eliminating the need for human intervention. In practice, the use of robot can be replaced by humans carrying mobile devices, because the WiFi chip of the mobile device can also collect CSI, and the IMU equipped with it can realize the measurement of itself rotation. For example, in such a scenario, the person moves and rotates the handheld mobile device to collect test samples and estimate the antennas' orientations according to the prompts of the APP, which would implement our methods. In such case, we would need to give instructions to human operators (e.g., rotating the device in the direction indicated) and deal with static reflection

paths (e.g., humans can choose LoS subjectively), but there are also benefits, such as no NLoS identification. We plan to extend these in future work.

**Diverse NLoS scenarios.** In this paper, we evaluate two NLoS conditions. In the real-world, concrete pillars and wooden boards are two common types of obstacles, which are also widely present in many new scenarios. Therefore, our threshold-based NLoS identification scheme is still applicable to many new scenarios. Additionally, *Anteumbler* can utilize other devices and technologies to assist in obstacle measurement, such as Lidar and video. However, these devices are not effective in estimating the orientation of the AP antenna. To address diverse NLoS scenarios, we are investigating other types of obstacles that might affect antenna orientation estimation, including metal walls, glass windows, and vegetation. By comprehensively considering these factors, we hope to enhance the robustness of the system in complex environments.

**Diverse antennas and WiFi NICs.** In this paper, we use *Linux 802.11n CSI Tool* [46] on the IWL5300 NIC to collect CSI. Currently, there are other tools available that support obtaining CSI from various WiFi nNICs, such as *Atheros CSI tool* [56], *Nexmon CSI Extractor* [57], and *PicoScenes* [58]. In fact, our antenna orientation search algorithm does not depend on CSI characteristics, with potential differences only in the CSI processing. We plan to analyze the CSI of more WiFi NICs in future work to extend the applicability of our system. Additionally, we plan to continue deploying and testing different models and sizes of linearly polarized antennas to validate the robustness of *Anteumbler*.

## IX. RELATED WORK

### A. WiFi-based Localization

Due to its ubiquitous deployment, WiFi has been extensively studied for indoor localization and tracking in the past two decades. Some of the initial work is based on RSSI [59]–[61], but these algorithms usually require a lot of fingerprint to achieve decimeter-level localization accuracy. Therefore, most recent works focus on localization algorithms based on fine-grained CSI [2]–[4], [62]–[66], and their commonly used localization ideas include AoA-based [2], [3], ToF-based [64], and fusion of AoA and ToF [1]. Many systems can achieve decimeter-level localization accuracy using commercial WiFi devices. However, these WiFi-based localization systems do not take into account the effects of APs' or antennas' orientation errors, they assume that the APs' and antennas' orientations are precisely known and parallel to ensure accurate antenna separation for estimating user location. Compared with the above works, we quantitatively analyze the effect of APs' or antennas' orientation errors on localization accuracy, and construct an antenna orientation estimation method that can accurately estimate the orientation of each antenna on the AP. The accuracy of the localization system is guaranteed by correction the antenna orientation.

### B. Reverse Localization of WiFi AP

WiFi-based localization systems assume accurate knowledge of AP locations, orientations and antenna geometry, but in the real world, these AP attribute information is often unknown or inaccurate, making WiFi localization difficult to deploy [24]. Reverse localization is designed to solve this problem by obtaining AP attribute information autonomously. There are some works on the reverse localization of WiFi AP [24], [25], [60], [67]. LocAP [24] systematically analyzes the influence of spatial attributes such as AP's location, orientation and antenna separation on the localization accuracy, and based on the SLAM robot, it realizes autonomous mapping of these spatial attributes of APs in unknown physical maps. MapFi [25] proposes an estimation method of *angle difference of arrival* (ADoA) for many heterogeneous WiFi APs and various antenna layouts. It only needs to know the locations of three APs in advance, so that APs with different antenna layouts can locate each other without additional equipment. However, they can only measure different orientations of APs in the horizontal plane, and they all assume that all antennas on the AP are parallel. In contrast to these works, *Anteumbler* estimates the orientation of each antenna, which in turn ensures the accuracy of WiFi AP reverse localization.

### C. Estimation of Antenna Orientation or Tilt Angle

Traditionally, there are some methods to estimate the elevation and azimuth angles of the antenna. For example, the antenna orientation is manually measured or calibrated using a compass [27] or inclinometer [68]. There are also integrated systems on the antenna that can measure the antenna orientation [28], [29]. But these are labor intensive or require the antenna to be equipped with sensors. In addition, vision-based method requires sufficient lighting for the antennas to be observed [30]. In this paper, we non-invasively estimate antennas' orientations (elevation and azimuth angles) based on commercial WiFi signals. To the best of our knowledge, *Anteumbler* is the first attempt to estimate antenna elevation and azimuth angles based on commercial WiFi signals.

## X. CONCLUSION

This paper presents the design and implementation of *Anteumbler*, the first attempt to measure the orientation of each AP antenna in physical space using WiFi signals. *Anteumbler* delivers two primary technical innovations. First, it incorporates a spatial angle model capable of estimating antenna orientation solely based on CSI provided by WiFi chips, without imposing additional requirements on the APs. Second, it integrates an optimization model that combines the orthogonality of electric field components, an iterative algorithm, and spatial geometry principle to achieve precise measurement of AP antenna orientations within minute-level time, while also mitigating the effects of propagation distance. Real-world experiments conducted across various antenna types, layouts, AP heights, and environmental conditions demonstrate that *Anteumbler* achieves median errors below $6°$ for both elevation and azimuth angles. By enabling accurate measurement of all AP antenna orientations, *Anteumbler* is poised to enhance the long-term accuracy of numerous WiFi-based localization and sensing systems in real-world applications.

## REFERENCES

[1] Y. Xie, J. Xiong, M. Li, and K. Jamieson, "md-track: Leveraging multi-dimensionality for passive indoor wi-fi tracking," in *The 25th Annual International Conference on Mobile Computing and Networking*, 2019, pp. 1–16.

[2] J. Xiong and K. Jamieson, "Arraytrack: A fine-grained indoor location system," in *10th USENIX Symposium on Networked Systems Design and Implementation (NSDI 13)*, 2013, pp. 71–84.

[3] M. Kotaru, K. Joshi, D. Bharadia, and S. Katti, "Spotfi: Decimeter level localization using wifi," *SIGCOMM Comput. Commun. Rev.*, vol. 45, no. 4, p. 269–282, aug 2015. [Online]. Available: https://doi.org/10.1145/2829988.2787487

[4] S. Kumar, S. Gil, D. Katabi, and D. Rus, "Accurate indoor localization with zero start-up cost," in *Proceedings of the 20th annual international conference on Mobile computing and networking*, 2014, pp. 483–494.

[5] H. Wang, D. Zhang, J. Ma, Y. Wang, Y. Wang, D. Wu, T. Gu, and B. Xie, "Human respiration detection with commodity wifi devices: Do user location and body orientation matter?" in *Proceedings of the 2016 ACM international joint conference on pervasive and ubiquitous computing*, 2016, pp. 25–36.

[6] J. Ma, Z. Chang, F. Zhang, J. Xiong, B. Jin, and D. Zhang, "Mobi2sense: enabling wireless sensing under device motions," in *Proceedings of the 28th Annual International Conference on Mobile Computing And Networking*, 2022, pp. 766–768.

[7] D. Huang, R. Nandakumar, and S. Gollakota, "Feasibility and limits of wi-fi imaging," in *Proceedings of the 12th ACM conference on embedded network sensor systems*, 2014, pp. 266–279.

[8] A. Pallaprolu, B. Korany, and Y. Mostofi, "Wiffract: a new foundation for rf imaging via edge tracing," in *Proceedings of the 28th Annual International Conference on Mobile Computing And Networking*, 2022, pp. 255–267.

[9] J. Wang, J. Xiong, X. Chen, H. Jiang, R. K. Balan, and D. Fang, "Tagscan: Simultaneous target imaging and material identification with commodity rfid devices," in *Proceedings of the 23rd Annual International Conference on Mobile Computing and Networking*, 2017, pp. 288–300.

[10] D. Yan, P. Yang, F. Shang, W. Jiang, and X.-Y. Li, "Wi-painter: Fine-grained material identification and image delineation using cots wifi devices," *Proceedings of the ACM on Interactive, Mobile, Wearable and Ubiquitous Technologies*, vol. 7, no. 4, pp. 1–25, 2024.

[11] D. Yan, P. Yang, F. Shang, N. M. Freris, and Y. Yan, "Anteumbler: Non-invasive antenna orientation error measurement for wifi aps," 2024. [Online]. Available: https://arxiv.org/abs/2408.11660

[12] F. Shang, P. Yang, Y. Yan, and X.-Y. Li, "Liqray: non-invasive and fine-grained liquid recognition system," in *Proceedings of the 28th Annual International Conference on Mobile Computing And Networking*, 2022, pp. 296–309.

[13] R. Gao, M. Zhang, J. Zhang, Y. Li, E. Yi, D. Wu, L. Wang, and D. Zhang, "Towards position-independent sensing for gesture recognition with wi-fi," *Proceedings of the ACM on Interactive, Mobile, Wearable and Ubiquitous Technologies*, vol. 5, no. 2, pp. 1–28, 2021.

[14] T. Manabe, Y. Miura, and T. Ihara, "Effects of antenna directivity and polarization on indoor multipath propagation characteristics at 60 ghz," *IEEE Journal on Selected Areas in Communications*, vol. 14, no. 3, pp. 441–448, 1996.

[15] J. Przewocki, M. J. Ammann, and A. Narbudowicz, "Measurement of orientation and distance change using circularly polarized uwb signals," *IEEE Transactions on Antennas and Propagation*, vol. 70, no. 6, pp. 4803–4809, 2022.

[16] C. Su, Y. Liu, L. Liu, M. Yang, H. Zhao, and X. Yin, "Experimental evaluation of multipath mitigation in tdoa-based indoor passive localization system using a beam steering broadband circular polarization antenna," *Electronics*, vol. 7, no. 12, 2018. [Online]. Available: https://www.mdpi.com/2079-9292/7/12/362

[17] N. Herscovivi and E. Dziadek, "Omnidirectional antennas for wireless communication," in *IEEE Antennas and Propagation Society International Symposium. 1999 Digest. Held in conjunction with: USNC/URSI National Radio Science Meeting (Cat. No.99CH37010)*, vol. 1, 1999, pp. 556–559 vol.1.

[18] Y. Schröder, T. Koke, C. Thomas, and L. Wolf, "Investigation of angle dependent errors in phase-based ranging with different antennas," in *Proceedings of the 2020 International Conference on Embedded Wireless Systems and Networks on Proceedings of the 2020 International Conference on Embedded Wireless Systems and Networks*, ser. EWSN '20. USA: Junction Publishing, 2020, p. 156–161.

[19] L. Chen, W. Hu, K. Jamieson, X. Chen, D. Fang, and J. Gummeson, "Pushing the physical limits of IoT devices with programmable metasurfaces," in *18th USENIX Symposium on Networked Systems Design and Implementation (NSDI 21)*. USENIX Association, Apr. 2021, pp. 425–438. [Online]. Available: https://www.usenix.org/conference/nsdi21/presentation/chen

[20] LifewiRe, "How to position router antennas," https://www.lifewire.com/ways-to-position-router-antennas-5206950, 2021.

[21] X. Wang, K. Niu, J. Xiong, B. Qian, Z. Yao, T. Lou, and D. Zhang, "Placement matters: Understanding the effects of device placement for wifi sensing," *Proceedings of the ACM on Interactive, Mobile, Wearable and Ubiquitous Technologies*, vol. 6, no. 1, pp. 1–25, 2022.

[22] M. Pelka, M. Cimdins, and H. Hellbrück, "Impact of the antenna orientation for distance estimation," *Proceedings of the 3rd KuVS/GI Expert Talk on Localization*, pp. 17–19, 2018.

[23] H. Schulten, M. Kuhn, R. Heyn, G. Dumphart, F. Trösch, and A. Wittneben, "On the crucial impact of antennas and diversity on BLE RSSI-based indoor localization," in *IEEE Vehicular Technology Conference (VTC Spring)*, Apr. 2019. [Online]. Available: http://www.nari.ee.ethz.ch/wireless/pubs/p/vtc2019antennas

[24] R. Ayyalasomayajula, A. Arun, C. Wu, A. Shaikh, S. Rajagopalan, Y. Hu, S. Ganesaraman, C. J. Rossbach, A. Seetharaman, E. Witchel *et al.*, "Locap: Autonomous millimeter accurate mapping of wifi infrastructure," in *17th USENIX Symposium on Networked Systems Design and Implementation (NSDI 20)*, 2020, pp. 1115–1129.

[25] X. Tong, H. Wang, X. Liu, and W. Qu, "Mapfi: Autonomous mapping of wi-fi infrastructure for indoor localization," *IEEE Transactions on Mobile Computing*, pp. 1–1, 2021.

[26] ASUS, "Asus wireless router," https://www.asus.com/support/FAQ/1030608/, 2022.

[27] Lindsay McIntosh-Tolle, "How to use a compass," https://www.rei.com/learn/expert-advice/navigation-basics.html, 2024.

[28] Digisat, "Cpi sat 2.4aebp 2.4m 2-axis elevation-over-azimuth," https://www.digisat.org/cpi-2.4aebp-antenna-positioner, 2022.

[29] C. I. Ngabo and O. El Beqqali, "3d tilt sensing by using accelerometer-based wireless sensor networks: Real case study: Application in the smart cities," in *2018 International Conference on Intelligent Systems and Computer Vision (ISCV)*. IEEE, 2018, pp. 1–8.

[30] Y. Yang, M. Wang, X. Wang, C. Li, Z. Shang, and L. Zhao, "A novel monocular vision technique for the detection of electric transmission tower tilting trend," *Applied Sciences*, vol. 13, no. 1, p. 407, 2022.

[31] H. T. Friis, "A note on a simple transmission formula," *Proceedings of the IRE*, vol. 34, no. 5, pp. 254–256, 1946.

[32] R. J. M. John D. Kraus, *Antenna: For All Application, Third Edition*. The McGraw-Hill Companies, Inc, 2002.

[33] P. Bevelacqua, "Friis equation-(aka friis transmission formula)," 2021.

[34] E. C. Jordan and K. G. Balmain, *Electromagnetic waves and radiating systems*. Prentice-Hall, 1968.

[35] D. K. Cheng *et al.*, *Field and wave electromagnetics*. Pearson Education India, 1989.

[36] X. Qing and Z. N. Chen, *Omnidirectional Antennas*. Singapore: Springer Singapore, 2014, pp. 1–53. [Online]. Available: https://doi.org/10.1007/978-981-4560-75-7_52-1

[37] W. Stutzman, "Estimating directivity and gain of antennas," *IEEE Antennas and Propagation Magazine*, vol. 40, no. 4, pp. 7–11, 1998.

[38] S. M. Bowers, A. Safaripour, and A. Hajimiri, "Dynamic polarization control," *IEEE Journal of Solid-State Circuits*, vol. 50, no. 5, pp. 1224–1236, 2015.

[39] U. M. Khan and M. Shahzad, "Estimating soil moisture using rf signals," in *Proceedings of the 28th Annual International Conference on Mobile Computing And Networking*, 2022, pp. 242–254.

[40] D. Yan, Y. Yan, P. Yang, W.-Z. Song, X.-Y. Li, and P. Liu, "Real-time identification of rogue wifi connections in the wild," *IEEE Internet of Things Journal*, vol. 10, no. 7, pp. 6042–6058, 2022.

[41] F. Benedetto, G. Giunta, A. Toscano, and L. Vegni, "Dynamic los/nlos statistical discrimination of wireless mobile channels," in *2007 IEEE 65th Vehicular Technology Conference-VTC2007-Spring*. IEEE, 2007, pp. 3071–3075.

[42] Z. Zhou, Z. Yang, C. Wu, W. Sun, and Y. Liu, "Lifi: Line-of-sight identification with wifi," in *IEEE INFOCOM 2014-IEEE Conference on Computer Communications*. IEEE, 2014, pp. 2688–2696.

[43] C. Wu, Z. Yang, Z. Zhou, K. Qian, Y. Liu, and M. Liu, "Phaseu: Real-time los identification with wifi," in *2015 IEEE conference on computer communications (INFOCOM)*. IEEE, 2015, pp. 2038–2046.

[44] X. Niu, S. Li, Y. Zhang, Z. Liu, D. Wu, R. C. Shah, C. Tanriover, H. Lu, and D. Zhang, "Wimonitor: Continuous long-term human vitality

This article has been accepted for publication in IEEE Transactions on Mobile Computing. This is the author's version which has not been fully edited and content may change prior to final publication. Citation information: DOI 10.1109/TMC.2024.3485228

15

monitoring using commodity wi-fi devices," *Sensors*, vol. 21, no. 3, p. 751, 2021.

[45] Y. Zeng, D. Wu, J. Xiong, E. Yi, R. Gao, and D. Zhang, "Farsense: Pushing the range limit of wifi-based respiration sensing with csi ratio of two antennas," *Proc. ACM Interact. Mob. Wearable Ubiquitous Technol.*, vol. 3, no. 3, sep 2019. [Online]. Available: https://doi.org/10.1145/3351279

[46] D. Halperin, W. Hu, A. Sheth, and D. Wetherall, "Tool release: Gathering 802.11n traces with channel state information," *ACM SIGCOMM CCR*, vol. 41, no. 1, p. 53, Jan. 2011.

[47] UMot, "Umot motor," http://www.umotmotor.com/, 2022.

[48] Schutt, "Schutt absorbing materials," http://en.xiate.net/index.php?m=Product&a=index&id=29, 2022.

[49] Gyroscope, "Gyroscope," http://wit-motion.com/, 2022.

[50] TurtleBot, "Turtlebot," https://www.turtlebot.com/, 2022.

[51] Hokuyo, "Hokuyo," https://www.hokuyo-aut.jp/, 2022.

[52] Gmapping, "Gmapping," http://wiki.ros.org/gmapping, 2022.

[53] S. Best, "Distance-measurement error associated with antenna phase-center displacement in time-reference radio positioning systems," *IEEE Antennas and Propagation Magazine*, vol. 46, no. 2, pp. 13–22, 2004.

[54] H. Zhang, Y. Guo, and G. Wang, "A wideband circularly polarized crossed-slot antenna with stable phase center," *IEEE Antennas and Wireless Propagation Letters*, vol. 18, no. 5, pp. 941–945, 2019.

[55] HCJYET, "Hcjyet," http://www.hcjyet.com/, 2022.

[56] Y. Xie, Z. Li, and M. Li, "Precise power delay profiling with commodity wifi," in *Proceedings of the 21st Annual international conference on Mobile Computing and Networking*, 2015, pp. 53–64.

[57] F. Gringoli, M. Schulz, J. Link, and M. Hollick, "Free your csi: A channel state information extraction platform for modern wi-fi chipsets," in *Proceedings of the 13th International Workshop on Wireless Network Testbeds, Experimental Evaluation & Characterization*, 2019, pp. 21–28.

[58] Z. Jiang, T. H. Luan, X. Ren, D. Lv, H. Hao, J. Wang, K. Zhao, W. Xi, Y. Xu, and R. Li, "Eliminating the barriers: Demystifying wi-fi baseband design and introducing the picoscenes wi-fi sensing platform," *IEEE Internet of Things Journal*, vol. 9, no. 6, pp. 4476–4496, 2021.

[59] P. Bahl and V. Padmanabhan, "Radar: an in-building rf-based user location and tracking system," in *Proceedings IEEE INFOCOM 2000. Conference on Computer Communications. Nineteenth Annual Joint Conference of the IEEE Computer and Communications Societies (Cat. No.00CH37064)*, vol. 2, 2000, pp. 775–784 vol.2.

[60] K. Chintalapudi, A. Padmanabha Iyer, and V. N. Padmanabhan, "Indoor localization without the pain," in *Proceedings of the Sixteenth Annual International Conference on Mobile Computing and Networking*, ser. MobiCom '10. New York, NY, USA: Association for Computing Machinery, 2010, p. 173–184. [Online]. Available: https://doi.org/10.1145/1859995.1860016

[61] X. Zhu, Y. Feng *et al.*, "Rssi-based algorithm for indoor localization," *Communications and Network*, vol. 5, no. 02, p. 37, 2013.

[62] J. Gjengset, J. Xiong, G. McPhillips, and K. Jamieson, "Phaser: Enabling phased array signal processing on commodity wifi access points," in *Proceedings of the 20th Annual International Conference on Mobile Computing and Networking*, ser. MobiCom '14. New York, NY, USA: Association for Computing Machinery, 2014, p. 153–164. [Online]. Available: https://doi.org/10.1145/2639108.2639139

[63] E. Soltanaghaei, A. Kalyanaraman, and K. Whitehouse, "Multipath triangulation: Decimeter-level wifi localization and orientation with a single unaided receiver," in *Proceedings of the 16th Annual International Conference on Mobile Systems, Applications, and Services*, ser. MobiSys '18. New York, NY, USA: Association for Computing Machinery, 2018, p. 376–388. [Online]. Available: https://doi.org/10.1145/3210240.3210347

[64] D. Vasisht, S. Kumar, and D. Katabi, "Decimeter-level localization with a single wifi access point," in *Proceedings of the 13th Usenix Conference on Networked Systems Design and Implementation*, ser. NSDI'16. USA: USENIX Association, 2016, p. 165–178.

[65] J. Xiong, K. Sundaresan, and K. Jamieson, "Tonetrack: Leveraging frequency-agile radios for time-based indoor wireless localization," in *Proceedings of the 21st Annual International Conference on Mobile Computing and Networking*, ser. MobiCom '15. New York, NY, USA: Association for Computing Machinery, 2015, p. 537–549. [Online]. Available: https://doi.org/10.1145/2789168.2790125

[66] J. Wang, H. Jiang, J. Xiong, K. Jamieson, X. Chen, D. Fang, and B. Xie, "Lifs: Low human-effort, device-free localization with fine-grained subcarrier information," in *Proceedings of the 22nd Annual International Conference on Mobile Computing and Networking*, 2016, pp. 243–256.

[67] Z. Chen, X. Tong, and X. Tian, "Deriving ap position and antenna array orientation for wi-fi localization," in *2019 11th International Conference on Wireless Communications and Signal Processing (WCSP)*, 2019, pp. 1–7.

[68] STRAINSENSE, "Inclinometer sensors / tilt sensors," https://www.strainsense.co.uk/sensors/position/inclinometers-tilt/, 2024.
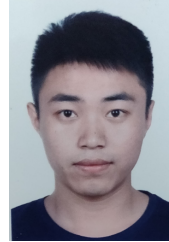
**Dawei Yan** received the BS degree in engineering from the School of Instrument Science and Electrical Engineering, Jilin University, China, in 2016. He is currently working toward the PhD degree with the University of Science and Technology of China. His current research interests include mobile computing and wireless sensing.

**Panlong Yang** (Senior Member, IEEE) received the BS, MS, and PhD degrees in communication and information system from the Nanjing Institute of Communication Engineering, China, in 1999, 2002, and 2005 respectively. He is now a professor with Nanjing University of Information Science & Technology. His research interests include wireless mesh networks, wireless sensor networks, and cognitive radio networks. He is a member of the IEEE Computer Society and ACM SIGMOBILE Society.

**Fei Shang** received the BS degree in electronic information engineering from the College of Information Science and Technology, Northwest University, China, in 2020. He is currently working toward the PhD degree with the University of Science and Technology of China. His current research interests include wireless sensing systems, wireless networks, and IoT Technology.

**Nikolaos M. Freris** (Senior Member, IEEE) received the Diploma in electrical and computer engineering from the National Technical University of Athens (NTUA), Athens, Greece, in 2005, and the MS degree in ECE, the MS degree in mathematics, and the PhD degree in ECE from the University of Illinois at Urbana-Champaign (UIUC), Champaign, IL, USA, in 2007, 2008, and 2010, respectively. He is currently a professor with the School of Computer Science and Technology and the Vice Dean of the International College, University of Science and Technology of China (USTC), Hefei, China. He was with the faculty of NYU and, before that, he held Senior Researcher and Postdoctoral Researcher positions at EPFL and IBM Research, respectively. He has authored or co-authored several papers in high-profile conferences and journals by IEEE, ACM, and SIAM, and he holds three patents. His research interests include AIoT/CPS/IoT, machine learning, distributed optimization, data mining, wireless networks, control, and signal processing, with applications in power systems, sensor networks, transportation, cyber security, and robotics.

**Yubo Yan** (Member, IEEE) received the BS, MS, and PhD degrees in communication and information system from the PLA University of Science and Technology, China, in 2006, 2011 and 2017 respectively. He is now an associate professor with the University of Science and Technology of China. His current research interests include Internet of Things, wireless networks, intelligent sensing, and mobile computing. He is a member of the IEEE Communications Society.